RSC Advances

PAPER

View Article Online
View Journal | View Issue

Cite this: *RSC Adv.*, 2022, **12**, 29162

Qualifying the contribution of fiber diameter on the acrylate-based electrospun shape memory polymer nano/microfiber properties†

Jiaxin Xi, Shima Shahab and Reza Mirzaeifar *

Received 10th August 2022
Accepted 25th September 2022

DOI: 10.1039/d2ra05019f

rsc.li/rsc-advances

Fibrous shape memory polymers (SMPs) have received growing interest in various applications, especially in biomedical applications, which offer new structures at the microscopic level and the potential of enhanced shape deformation of SMPs. In this paper, we report on the development and investigation of the properties of acrylate-based shape memory polymer fibers, fabricated by electrospinning technology with the addition of polystyrene (PS). Fibers with different diameters are manufactured using four different PS solution concentrations (25, 30, 35, and 40 wt%) and three flow rates (1.0, 2.5, and 5.0 μL min^{-1}) with a 25 kV applied voltage and 17 cm electrospinning distance. Scanning electron microscope (SEM) images reveal that the average fiber diameter varies with polymer concentration and flow rates, ranging from 0.655 ± 0.376 to 4.975 ± 1.634 μm. Dynamic mechanical analysis (DMA) and stress–strain testing present that the glass transition temperature and tensile values are affected by fiber diameter distribution. The cyclic bending test directly proves that the electrospun SMP fiber webs are able to fully recover; additionally, the recovery speed is also affected by fiber diameter. With the combination of the SMP material and electrospinning technology, this work paves the way in designing and optimizing future SMP fibers properties by adjusting the fiber diameter.

1. Introduction

Shape memory polymers (SMPs) are a relatively new kind of stimuli-responsive materials that provide the ability to store one or more temporary shapes and return to their original permanent shape under an external stimulus.[1–3] The external stimuli include heat,[4,5] magnetism,[6,7] pH,[8,9] light,[10,11] moisture,[12] and focused ultrasound.[13,14] In the past several years, SMPs have received extended attention because of their flexibility,[15] low cost[16] and lightweight,[17] as well as easy processability.[18] Because of these advantages, SMPs display promising applications in various fields: soft actuators and robotics,[7,19] aerospace,[20] tissue engineering,[21] and biomedicine.[22] Recently, nano/microfibers have become more attractive due to their small size and flexible materials, showing a trend of broader applicability in the biomedical field, such as in tissue engineering,[23] artificial muscles,[24] drug release,[25] smart clothing,[26,27] and scaffolds.[28] However, SMP-based nanostructures have not been well explored, especially in terms of fabrication techniques and properties affected by sizes. Thus, it is of great significance to study SMPs' fiber structure.

Fibrous SMPs are of great interest for structural and functional applications due to their high surface area-to-volume ratio, high degree of porosity with tiny pore size, and 3D architectures that resemble extracellular matrices.[29–32] The SMP nanofibers can be fabricated by the electrospinning method. Electrospinning method simply and efficiently constructs continuous polymer ultrafine fibers using an electric field placed on a polymer solution or melt.[29,33,34] Electrospun several functional materials have recently been used in various application fields. Budun *et al.*[35] fabricated shape memory polyurethane (SMPU) fibers (112 ± 34 to 2046 ± 654 nm), which were triggered by heat with a shape recovery rate of above 100%. Zhang *et al.*[36] reported SMPU spent only one-fourth of the shape recovery time of that used for bulk film when heated in a water bath. Matsumoto *et al.*[37] reported microscale non-woven fabrics fabricated from poly(*x*-pentadecalactone) (PPDL) and poly(*e*-caprolactone) (PCL), which displayed good shape memory ability after muti-thermomechanical tensile tests, and which had potential application in biomedicine. In addition, some novel two-way or multiple SMP composites fibers were produced by introducing different fillers or synthesized by some special groups with reversible shape deformation.[38,39]

Acrylate-based shape memory polymer owning biocompatibility[40,41] may be a promising candidate for use in biomedical adapting to a diverse range of applications. In our group, Bhargava *et al.*[13,42,43] used *tert*-butyl acrylate (*t*BA) and di(ethylene glycol) dimethacrylate (DEGMA) to synthesize SMPs. They reported how the ratio of *t*BA (monomer) to DEGMA (crosslinker) affects the shape memory, and measured the highest recovery ratio to be about 20% by changing the composition

Department of Mechanical Engineering, Virginia Tech, Blacksburg, Virginia 24061, USA. E-mail: rmirzaei@vt.edu; Web: https://www.futurematerials-lab.com/; Fax: +1-540-231-2903; Tel: +1-540-231-8697

† Electronic supplementary information (ESI) available. See DOI: https://doi.org/10.1039/d2ra05019f

ratio. In another work by our group, Peng and co-workers[44] added polystyrene (PS) into *t*BA-*co*-DEGMA SMP matrix that exhibited almost 100% shape recovery in 2 seconds. In this SMP mixture, PS showed a significant effect on the shape recoverability and mechanical properties due to the change in the polymerization and crosslinking ratio throughout the curing process. Antony *et al.*[45] reported a new type of SMPs by using *t*BA and poly(ethylene glycol) dimethacrylate (PEGDMA) that can recover in 45 seconds after being heated in 55 °C hot water. With the addition of diurethane dimethacrylate (DUDMA), this SMP network fully recovered in around 20 seconds. And then, they introduced grafted hydroxyapatite into prepared *t*BA-*co*-PEGDMA. Grafted Hap with PEGMA significantly impacts the shape recoverability of system due to avoidance agglomeration and improvement of the interfacial interactions of the particles.[46] Among multiple types of SMPs, acrylate-based SMPs shows a three-dimensional/four-dimensional (3D/4D) printability.[47,48] Wu *et al.*[49] demonstrated a new 4D printable *tert*-butyl acrylate (*t*BA)-*co*-1, 6-hexanediol diacrylate (HDDA), which can be printed by using digital light processing with complex geometry. Choong *et al.*[50] developed stereolithography apparatus (SLA) to fabricate *tert*-butyl acrylate (*t*BA)-*co*-di(ethylene glycol) dimethacrylate (DEGMA) SMP. Recently, to the best of our knowledge, all of the mentioned acrylate-based shape memory systems are thin films; a shape memory nano/micro-composite fiber based on acrylate has not yet been studied; thus, this contribution represents a benchmark study to manufacture acrylate-based SMPs fiber using the electrospinning technique. The direct introduction of *t*BA as monomers and DEGMA as crosslinker in the electrospinning process is not possible due to their low molecular weight, meaning that they have very low viscosity. Thus, introducing of *t*BA-*co*-DEGMA (*t*D) in the fiber requires the use of an extra component, which is non-resorbable and biocompatible polystyrene (PS) with the high molecular weight. Therefore, we successfully manufacture *t*D/PS fibers using the electrospinning technique.

It is noted that specific properties of polymer nanofiber are significantly different from those in bulk.[32,51] Moreover, polymer fibers display unique size-dependent mechanical properties, which are strongly related to the shape-memory properties.[52] The diameter significantly influences electrospun fibers' mechanical properties due to the core–shell structure and chain alignment.[32]

In this work, acrylate-based SMP fibers are successfully manufactured using electrospinning methods. The fabricated SMP fibers are characterized *via* scanning electron microscope (SEM) to investigate the morphological properties of these fibers. The SM effect is investigated with different fiber diameters. In addition, standard tensile tests, DMA analysis, shape fixity, and shape recovery tests are utilized to deeply evaluate the characteristics of fiber diameter property relationship.

2. Materials and methods

2.1. Solution preparation

Prior to prepare electrospun *tert*-butyl acrylate (*t*BA)-*co*-di(ethylene glycol) dimethacrylate (DEGMA) SMP and polystyrene (PS) mixture, the PS pellets (M_w = 35 000, Sigma-Aldrich, Inc.) are dissolved in the toluene (anhydrous, 99.8%; Sigma-Aldrich, Inc.), heated to 50 °C and stirred for 2 hours until PS pellets fully dissolved, in order to prepare the polymer concentration of 25, 30, 35 and 40 wt% PS solutions. The *t*BA (Sigma-Aldrich, Inc.) and DEGMA (Sigma-Aldrich, Inc.) are mixed at a weight ratio of 85 : 15, followed by adding 1 wt% photoinitiator 2,2-dimethoxy-2-phenyl-acetophenone (Sigma-Aldrich, Inc.) into the solution. Both PS and *t*BA-*co*-DEGMA (*t*D) solutions are mixed (50 : 50 w/w%), and then stirred for another 20 min to obtain homogeneous *t*D/PS solutions for electrospinning. More details of the synthesis method can be found in our previous publication.[44] The chemical structure is shown in Fig. 1a and b.

2.2. Electrospinning process

The electrospinning process is shown in Fig. 1c. The electrospinning setup included a syringe pump (CMA-Harvard Apparatus 4004 Syringe Pump, USA) connected with a 10 mL syringe, a high voltage power supply (DongWen High Voltage Power Supply; TianJin, China) and a rotational collector. The needle tip is subjected to the positive electrode; the collector is connected to the negative electrode. The working distance between the tip of the syringe and the collector is determined at 17 cm and the rotational speed of the collector is fix as 60 rpm. Electrospun fibers are collected on the surface of cleaned aluminum foils, and then are cured with 365 nm UV light (with a 100 W Blak-Ray B-100 AP High Intensity UV Lamp) for 15 min. The prepared samples are post-dried inside the fume hood for 24 h. Three different flow rates are chosen: 1.0; 2.5; and 5.0 μL min^{-1}. Details of the electrospinning conditions of each specimen are listed in Table S1.†

2.3. SEM analysis of electrospun fibers

The morphology of electrospun fibers is observed by scanning electron microscope (JEOL IT-500HR SEM) at an accelerating voltage of 5 kV. All samples are firstly coated with a platinum/lead layer using a sputter coater with a thickness of 7.0 nm. The average fiber diameters are calculated for at least 200 fibers using the Image J software (Image J, 2021) from the SEM images at magnifications of 2500×.

2.4. Thermal and mechanical characterization

Specimens are prepared as 5 × 10 × 0.04 mm in size to determine the thermal and mechanical properties. The storage modulus for each sample is measured by dynamic mechanical analyzer (Q800 DMA, TA Instruments). The temperature is swept from 25 °C to 100 °C with a constant heating rate of 2 °C per minute, using an oscillation rate of 1 Hz. The mechanical properties of the samples are also measured by DMA Q800. The tensile tests of the samples obtained with different samples are performed at room temperature (*i.e.*, 25 °C). During the testing, a strain rate of 0.000167 s^{-1} (displacement control) is applied to the specimens. Three repetitions of each test are taken for each specimen.

2.5. Shape memory property

Fig. 2 displays the schematic diagram of the bending test process. Specimens used to determine the shape memory effect

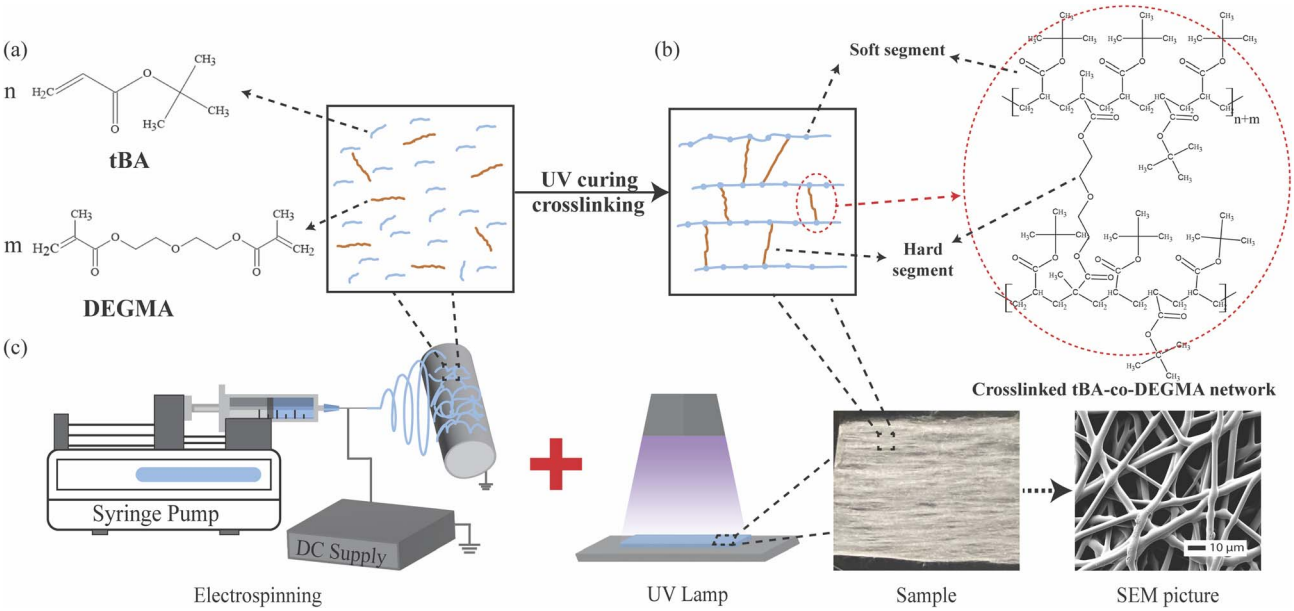

Fig. 1 (a) Chemical structures of *t*BA (monomer) and DEGMA (crosslinker); (b) UV curing forms the permanent crosslinked *t*BA-*co*-DEGMA network; (c) schematic of the electrospinning process with UV curing: syringe pump, DC supply and rotational collector; UV lamp; sample image; and SEM image. Details of the procedure are given in Section 2.2 and Table S1.†

are prepared as 10 × 20 × 0.04 mm dimension. The bending test is not ideal because the strain in the bent area is not uniform;[53] however, it is a frequent testing method for quantifying the performance of shape deformation. In this work, we employ a bending test and record the change in bending angle to describe each sample's shape recovery capabilities. The flat specimen ($\theta_0 = 0°$) is heated to 70 °C by hot plate, and then bent to a U-shaped structure ($\theta_u = 180°$) using the curvature diameter of 3.5 mm in the tip. Secondly, the bent specimen is rapidly cooled down to room temperature in air (about 25 °C). The external force is removed, and then specimen is deformed freely. Afterwards, final fixed angle (θ_f) is measured after 30 min. Finally, the bent specimen is heated to 70 °C again, and the recovery angle (θ_r) is recorded using slow-motion camera and measured *via* an online protractor. To ensure the repeatability, at least three individual samples are tested. The temporary shape fixity ratio (R_f) and shape recovery ratio (R_r) equations are given as[54]

$$R_f(\%) = \frac{\theta_u - \theta_f}{\theta_u} \times 100\% \quad (1)$$

$$R_r(\%) = \frac{\theta_u - \theta_r}{\theta_u - \theta_0} \times 100\% \quad (2)$$

3. Results and discussions

3.1. Morphology and fiber diameter

In the electrospinning process, the fiber structure and morphology can be adjusted, and the fiber diameters can be aimed at a wide range of sizes, by optimized solution properties (polymer and solvent type, polymer concentration, viscosity, conductivity, molecular weight, *etc.*), process parameters (applied voltage, stock solution flow rate, and working distance between needle tip and collector, *etc.*) and ambient atmosphere (temperature and humidity).[29,55] In this work, mainly solution concentration and stock solution flow rate have been focused on, in order to study the effect of fiber diameter and morphology on the properties of electrospun fibers. Fig. 3 shows selected SEM images which reveal that the morphology of *t*D/PS SMP fibers varies with polymer concentration and flow rate. At *t*D/PS (25 wt%) system, fibers show beads-on-string morphologies and very small diameters. Electrospun *t*D/PS (30 wt%) fibers resulted in beaded fibers at flow ratio of 1.0 and 2.5 μL min^{-1}, and in smooth fiber at flow ratio of 5.0 μL min^{-1}. Electrospun *t*D/PS (35 and 40 wt%) fibers result in fairly smooth fibers. The bead density reduces with increasing polymer concentration. When polymer concentration is above 35%,

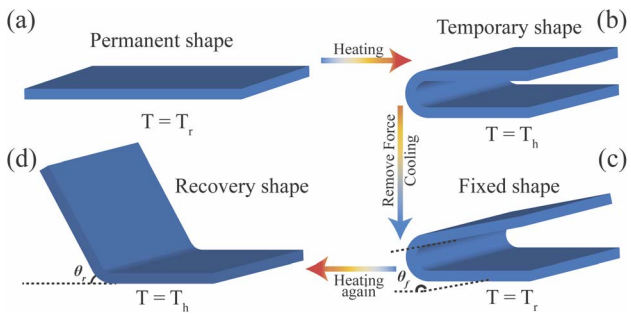

Fig. 2 Schematic of shape programming in bending deformation. (a) Permanent shape: flat shape; (b) temporary shape: U-shape after heating and bending; (c) fixed shape after releasing force and cooling down; (d) recovery shape during heating. More details of the procedure are given in Section 2.5.

smooth fibrous structures without beads are formed. The solution's viscoelasticity and surface tension, as well as the charge density carried by the jet, are important elements in the creation of beads.[56] It is known that the bead density decreases with increasing viscosity and net charge density, while decreasing surface tension. The solution viscosity in our case is tuned by adjusting the polymer concentration. The previous study reports that to enable the consistent and uniform fiber formation, a minimum polymer concentration is needed.[57] When the concentrations are below minimum (in our case, 35 wt%), the electrospinning process only could keep for a shorter time under a steady state. Additionally, Fig. 3 shows that the fibers obtained from the 5.0 L min^{-1} flow-rate sample, are stuck together, and remained moist in some spots. The reason behind of it is that not enough drying time for polymer solution before arriving at the collector and low stretching forces.[58]

The diameter ranges of electrospun fibers of *t*D/PS (35 wt%) at a flow rate of 1.0 μL min^{-1} are shown in Fig. 4a, S1 and S2.† Each range of diameter is large, which means that coarser and finer fibers are yielded together under the same electrospinning condition. This is due to few polymer jets splitting during the travelling to the collector, and then finer fibers are produced.

Fig. 4b and c display the average fiber diameter from each condition obtained from the electrospinning process. The smallest diameter (0.655 ± 0.376 μm) and beads-on-string fibers are belonged to the sample *t*D/PS (25 wt%) with a flow rate of 1.0 μL min^{-1}. Besides, the largest fiber diameter (4.975 ± 1.634 μm)

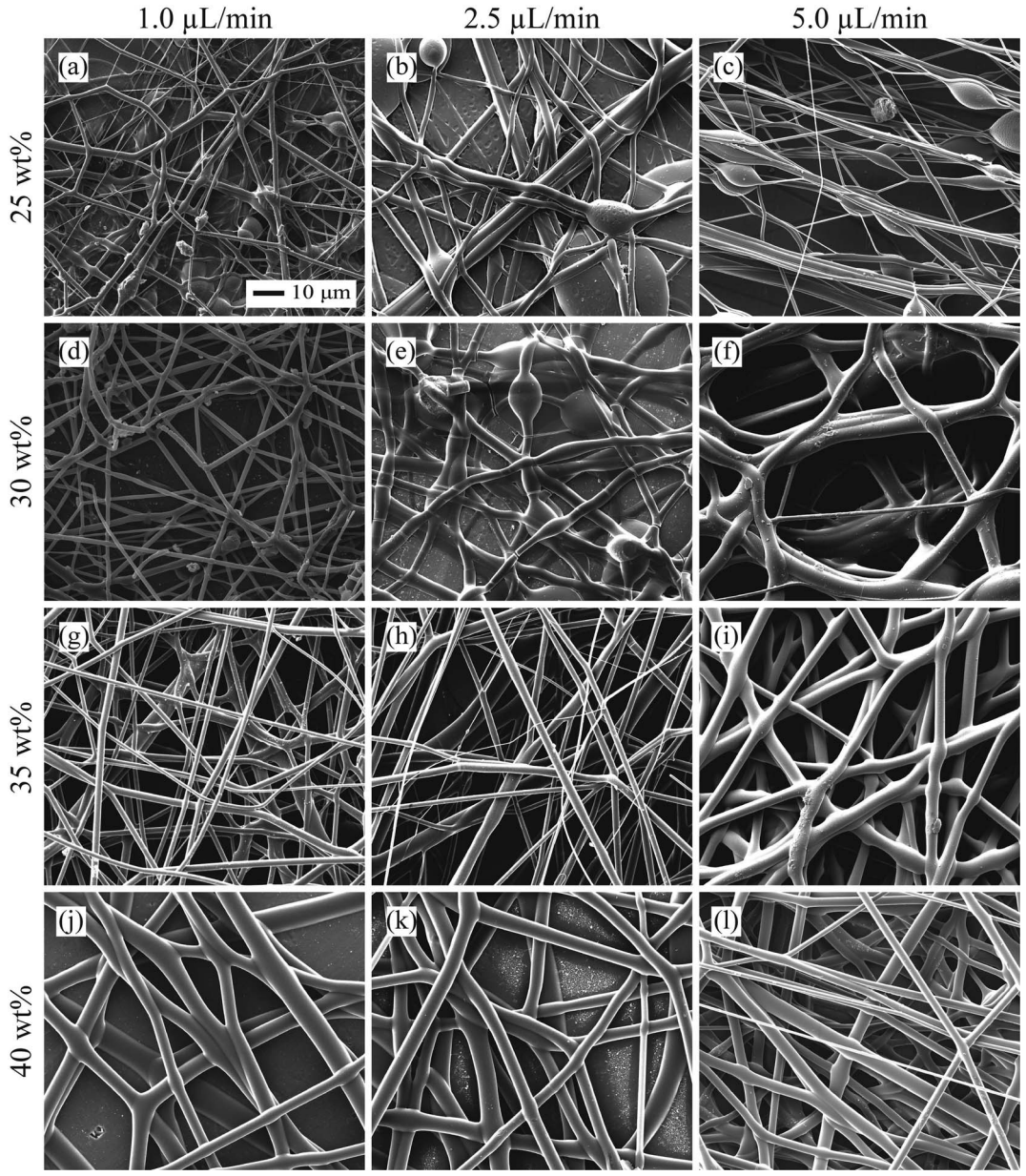

Fig. 3 SEM pictures (×1K magnification) of SMP electrospun fibers with different PS solution concentrations of 25 wt% (a–c), 30 wt% (d–f), 35 wt% (g–i) and 40 wt% (j–l) at various flow rates of 1.0 μL min^{-1} (a, d, g, j), 2.5 μL min^{-1} (b, e, h, k) and 5.0 μL min^{-1} (c, f, i, l).

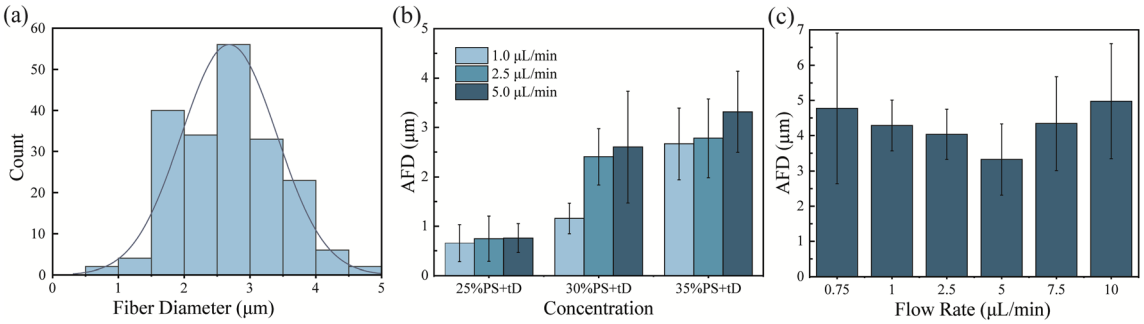

Fig. 4 (a) Histogram of fiber diameter distribution of electrospun fibers prepared with PS solution concentration of 35 wt% at a flow rate of 1.0 μL min^{-1}. Average fiber diameter of the SMP electrospun fibers with different PS solution concentrations at various flow rates, (b) *t*D/PS (25, 30, and 35 wt%), and (c) *t*D/PS (40 wt%).

and uniform fibers are obtained for *t*D/PS (40 wt%) with a flow rate of 10.0 μL min^{-1}. It is clearly shown that the fiber diameter increases with increasing the concentration due to higher viscosity. Greater electrical forces are needed to overcome surface tension and the viscoelastic force that causes fibers to stretch when the solution's viscosity is higher. Greater concentration results in fibers with a larger diameter when electrical force is equivalent. Similar to this, too high or too low concentrations could not be employed for electrospinning due to their excessive viscosity. At *t*D/PS (25, 30, and 35 wt%) systems, with increasing flow rate, the fiber diameter will increase. The common consideration is that the finer fiber diameters are generated at lower flow rates. The reason is that when the electrospinning jet's volume and starting radius grew, bending instability decreased and fiber diameter subsequently increased as a result. However, at *t*D/PS (40 wt%) system, with increasing flow rate, an initial increment in average fiber diameter is followed by an increment (Fig. 4c). This is caused by the emergence of secondary jets from the primary jet at flow ratios less than 5.0 μL min^{-1} as solidified solution at the nozzle's tip drives jet eruption from unsolidified surfaces.[59] When compared to the first main jet, the secondary jets will produce fibers with a lesser diameter. Additionally, secondary fibers generated from 7.5 and 10.0 μL min^{-1} flow-rate samples that stuck to the original main jet have probably been the cause of the enlargement in average fiber diameter with a high flow rate. The emergence of secondary jets from the primary jet as solidified solution at the tip of the nozzle pushes jet eruption from unsolidified surfaces has been explained as the cause of the decrease in average fiber diameter with flow rate. When compared to the first main jet, the secondary jets will produce fibers with a less diameter.

3.2. Thermomechanical and mechanical properties

SEM images for fiber morphologies show that *t*D/PS (35 wt%) system gives the most steady-state electrospinning with a flow rate from 1.0 to 5.0 μL min^{-1}, and it is used for all the future experiments in this paper. Shape memory electrospun *t*D/PS (35 wt%) webs are compared to each flow rate to determine the effect of the fiber diameter upon the glass transition temperature. Fig. S3† shows the thermal parameters derived by dynamic mechanical thermal analysis (DMA) for each fiber diameter. The overall thermomechanical properties of *t*D/PS (35 wt%) samples are dominated by the mixed phase, which has a wide glass transition temperature (T_g) range of 73 to 96 °C and thus allows the investigation of the SME with a variety of programming and recovery procedures, such as temperature memory properties. Glass transition temperature determined by the tan δ (see Fig. S3b†) maximum, Fig. 5 shows a T_g-increase is observed from 86.59 ± 0.5 °C, over 89.43 ± 1.65 °C and 92.18 ± 0.86 °C for the diameter reduction from 3.319 ± 0.825, over 2.782 ± 0.797 to 2.682 ± 0.726 μm. This result corresponds to experimental findings for electrospun polyetherurethane with diameters ranging from 2.3, over 1.0 to 0.3 μm.[60] This could be explained by the degree of crystallinity and degree of molecular orientation.[61]

The influence of the morphology and diameter of SMP fibers on the mechanical properties is also studied. The young's modulus of electrospun webs is displayed in Fig. 5. The load is dispersed and bared by the fibers when it is applied to the electrospun webs. This indicates that in order to achieve appropriate results in terms of mechanical qualities, the fibers should be produced uniformly lacking beads, more fibers should be obtained per unit area, and the size range of the fibers should

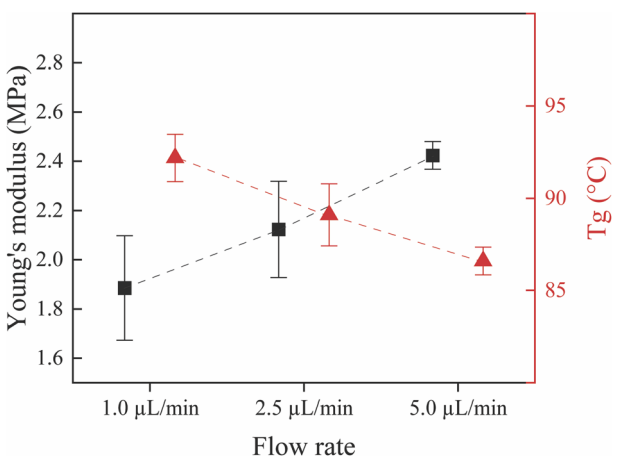

Fig. 5 Glass transition temperature (red triangles) and Young's modulus (black squares) of electrospun fibers with 35 wt% PS solution at various flow rates.

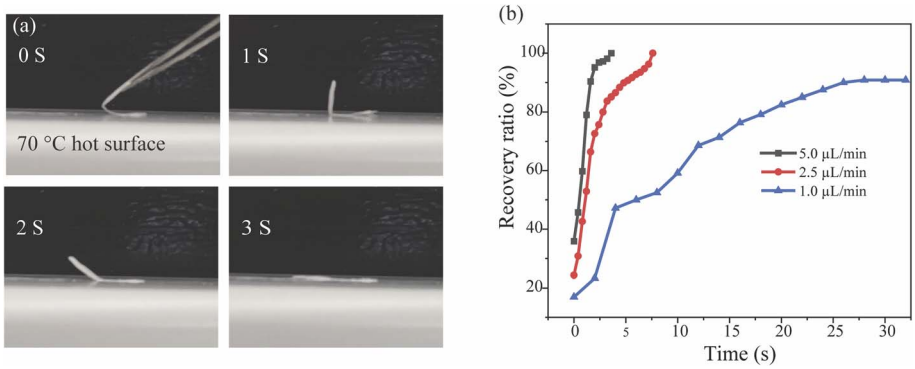

Fig. 6 (a) The digital images of the shape memory effect process of the bended *t*D/PS (35 wt%) electrospun web using 5 μL min^{-1} flow rate at 70 °C; (b) the shape recovery ratios as a function of the heating time for electrospun fibers with PS solution concentration of 35 wt% at various flow rates (1.0; 2.5 and 5.0 μL min^{-1}).

not be too broad. The greatest tensile property is obtained for *t*D/PS (35 wt%) at a flow ratio of 5.0 μL min^{-1} (2.45 ± 0.35 MPa). This sample has largest fiber diameters as well as most uniform structures. Although *t*D/PS (35 wt%) at a flow ratio of 5.0 μL min^{-1} had larger fiber diameter, but the size distribution of fiber is narrower. Fibers of *t*D/PS (35 wt%) at a flow ratio of 5.0 μL min^{-1} adhered and are crossed with each other called a cross-point. Chavoshnejad *et al.*[62] reported that the cross-point bonding increased the elastic modulus of the electrospun webs.

3.3. Shape-memory property

The influence of the diameter of the electrospun fiber on the shape recoverability is investigated. The thermally induced shape memory behavior of the bent electrospun web is illustrated in Fig. 6a and Video 1.† All samples exhibited the shape-memory effect, whereas an inverse relation between the temporary shape fixity ratio R_f towards the shape recovery ratio R_r is found (see Fig. 6b, as well as eqn (1) and (2) for definition of R_f and R_r). All gained shape fixity ratios are higher than 65% and the best result (91.1 ± 4%) is belong to *t*D/PS (35 wt%) at a flow ratio of 1.0 μL min^{-1}, which have the smallest diameter size. This is due to the high number of crossover sites between fibers, which allowed for more force to be carried more efficiently throughout fiber networks.[63] Conversely, all samples can achieve 100% shape recovery and the highest recovery speed is obtained for *t*D/PS (35 wt%) at a flow ratio of 5.0 μL min^{-1}, whose fiber diameter is the largest. It is because of the more amorphous domains included in its structures. Additionally, the inefficient evaporation during electrospinning process might have increased the shape recovery value of *t*D/PS (35 wt%) fiber using a flow ratio of 5.0 μL min^{-1}. In overall, increasing fiber diameter can enhance the shape recovery shape memory effect in terms of the response time and shape recoverability. Reversely, the shape fixity decreases.

4. Conclusions

In this study, a crosslinked acrylate-based shape memory polymer composite fibers have been successfully fabricated by using the electrospinning method with adding polystyrene (PS). The effect of polymer concentration and flow rate on the fiber diameter and morphology have been systematically studied. Our results show that the finer and more uniform fiber diameter is yielded from *t*D/PS (35 wt%) solution with three different flow rates (1.0, 2.5, and 5.0 μL min^{-1}) and an applied voltage of 25 kV at 17.0 cm distance. From corresponding tests, the structural characteristics and fiber diameters have significant effect upon the glass transition temperature and mechanical properties of the electrospun webs. All electrospun webs can reach 100% recovery ratio with above 65% shape fixity results. The shape memory results illustrate that the shape recovery and shape fixity properties of the electrospun webs are presumably affected by the fiber size and morphology. The obtained result will present multiple potential future applications. As an example, by optimizing the electrospinning parameters, the shape deformation can be controlled.

Conflicts of interest

There are no conflicts to declare.

Acknowledgements

Financial support from the NSF CMMI Grant 2016474 is gratefully acknowledged.

References

1 Y. He, S. Guo, Z. Liu and K. M. Liew, Pattern transformation of thermo-responsive shape memory polymer periodic cellular structures, *Int. J. Solids Struct.*, 2015, **71**, 194–205.
2 G. Scalet, Two-way and multiple-way shape memory polymers for soft robotics: an overview, *Actuators*, 2020, **9**, 10.
3 Y. Chi, Y. Li, Y. Zhao, Y. Hong, Y. Tang and J. Yin, Bistable and Multistable Actuators for Soft Robots: Structures, Materials, and Functionalities, *Adv. Mater.*, 2022, **34**(19), 2110384.
4 T. Gong, K. Zhao, W. Wang, H. Chen, L. Wang and S. Zhou, Thermally activated reversible shape switch of polymer particles, *J. Mater. Chem. B*, 2014, **2**(39), 6855–6866.

5 Y. Zhao, K. Peng, J. Xi, S. Shahab and R. Mirzaeifar, Achieving multimodal locomotion by a crosslinked poly(ethylene-co-vinyl acetate)-based two-way shape memory polymer, *Smart Mater. Struct.*, 2021, **31**(1), 015034.

6 Y. Cai, J.-S. Jiang, Z.-W. Liu, Y. Zeng and W.-G. Zhang, Magnetically-sensitive shape memory polyurethane composites crosslinked with multi-walled carbon nanotubes, *Composites, Part A*, 2013, **53**, 16–23.

7 Q. Ze, X. Kuang, S. Wu, J. Wong, S. M. Montgomery, R. Zhang, J. M. Kovitz, F. Yang, H. J. Qi and R. Zhao, Magnetic Shape Memory Polymers with Integrated Multifunctional Shape Manipulation, *Adv. Mater.*, 2020, **32**(4), 1906657.

8 X.-J. Han, Z.-Q. Dong, M.-M. Fan, Y. Liu, J.-H. li, Y.-F. Wang, Q.-J. Yuan, B.-J. Li and S. Zhang, pH-Induced Shape-Memory Polymers, *Macromol. Rapid Commun.*, 2012, **33**(12), 1055–1060.

9 Q. Song, H. Chen, S. Zhou, K. Zhao, B. Wang and P. Hu, Thermo- and pH-sensitive shape memory polyurethane containing carboxyl groups, *Polym. Chem.*, 2016, **7**(9), 1739–1746.

10 A. Lendlein, H. Jiang, O. Jünger and R. Langer, Light-induced shape-memory polymers, *Nature*, 2005, **434**(7035), 879–882.

11 M. Herath, J. Epaarachchi, M. Islam, L. Fang and J. Leng, Light Activated Shape Memory Polymers and Composites: A Review, *Eur. Polym. J.*, 2020, **136**, 109912.

12 S. Chen, J. Hu, C.-w. Yuen and L. Chan, Novel moisture-sensitive shape memory polyurethanes containing pyridine moieties, *Polymer*, 2009, **50**, 4424–4428.

13 A. Bhargava, K. Peng, J. Stieg, R. Mirzaeifar and S. Shahab, Focused ultrasound actuation of shape memory polymers; acoustic-thermoelastic modeling and testing, *RSC Adv.*, 2017, **7**(72), 45452–45469.

14 K. Peng, S. Shahab and R. Mirzaeifar, Interaction of high-intensity focused ultrasound with polymers at the atomistic scale, *Nanotechnology*, 2020, **32**(4), 045707.

15 J. Hu, Y. Zhu, H. Huang and J. Lu, Recent advances in shape–memory polymers: Structure, mechanism, functionality, modeling and applications, *Prog. Polym. Sci.*, 2012, **37**(12), 1720–1763.

16 C. Liu, H. Qin and P. T. Mather, Review of progress in shape-memory polymers, *J. Mater. Chem.*, 2007, **17**(16), 1543–1558.

17 W. Sokolowski, S. Tan, and M. Pryor, Lightweight Shape Memory Self-Deployable Structures for Gossamer Applications, in *45th AIAA/ASME/ASCE/AHS/ASC Structures, Structural Dynamics & Materials Conference*, American Institute of Aeronautics and Astronautics, 2004.

18 W. Sokolowski, A. Metcalfe, S. Hayashi, L. H. Yahia and J. Raymond, Medical applications of shape memory polymers, *Biomed. Mater.*, 2007, **2**(1), S23–S27.

19 C. Appiah, C. Arndt, K. Siemsen, A. Heitmann, A. Staubitz and C. Selhuber-Unkel, Living Materials Herald a New Era in Soft Robotics, *Adv. Mater.*, 2019, **31**(36), 1807747.

20 M. Zare, P. Davoodi and S. Ramakrishna, Electrospun Shape Memory Polymer Micro-/Nanofibers and Tailoring Their Roles for Biomedical Applications, *Nanomaterials*, 2021, **11**(4), 933.

21 R. Rošic, P. Kocbek, S. Baumgartner and J. Kristl, Electrospun hydroxyethyl cellulose nanofibers: the relationship between structure and process, *J. Drug Delivery Sci. Technol.*, 2011, **21**(3), 229–236.

22 W. t. Small, P. Singhal, T. S. Wilson and D. J. Maitland, Biomedical applications of thermally activated shape memory polymers, *J. Mater. Chem.*, 2010, **20**(18), 3356–3366.

23 D. Kai, M. P. Prabhakaran, B. Q. Chan, S. S. Liow, S. Ramakrishna, F. Xu and X. J. Loh, Elastic poly(ε-caprolactone)-polydimethylsiloxane copolymer fibers with shape memory effect for bone tissue engineering, *Biomed. Mater.*, 2016, **11**(1), 015007.

24 Q. Yang, J. Fan and G. Li, Artificial muscles made of chiral two-way shape memory polymer fibers, *Appl. Phys. Lett.*, 2016, **109**.

25 H. Lv, D. Tang, Z. Sun, J. Gao, X. Yang, S. Jia and J. Peng, Electrospun PCL-based polyurethane/HA microfibers as drug carrier of dexamethasone with enhanced biodegradability and shape memory performances, *Colloid Polym. Sci.*, 2020, **298**(1), 103–111.

26 Y. Zhong, F. Zhang, M. Wang, C. J. Gardner, G. Kim, Y. Liu, J. Leng, S. Jin and R. Chen, Reversible Humidity Sensitive Clothing for Personal Thermoregulation, *Sci. Rep.*, 2017, **7**, 44208.

27 J. Hu, H. Meng, G. Li and S. I. Ibekwe, A review of stimuli-responsive polymers for smart textile applications, *Smart Mater. Struct.*, 2012, **21**(5), 053001.

28 L. F. Tseng, P. T. Mather and J. H. Henderson, Shape-memory-actuated change in scaffold fiber alignment directs stem cell morphology, *Acta Biomater.*, 2013, **9**(11), 8790–8801.

29 R. Erdem, İ. Usta, M. Akalin, O. Atak, M. Yuksek and A. Pars, The impact of solvent type and mixing ratios of solvents on the properties of polyurethane based electrospun nanofibers, *Appl. Surf. Sci.*, 2015, **334**, 227–230.

30 R. Erdem and M. Akalın, Characterization and evaluation of antimicrobial properties of electrospun chitosan/polyethylene oxide based nanofibrous scaffolds (with/without nanosilver), *J. Ind. Text.*, 2013, **44**(4), 553–571.

31 Z. Ma, M. Kotaki, R. Inai and S. Ramakrishna, Potential of Nanofiber Matrix as Tissue-Engineering Scaffolds, *Tissue Eng.*, 2005, **11**(1–2), 101–109.

32 K. Peng, A. Nain and R. Mirzaeifar, Tracking the origins of size dependency in the mechanical properties of polymeric nanofibers at the atomistic scale, *Polymer*, 2019, **175**, 118–128.

33 H. Zhuo, J. Hu, S. Chen and L. Yeung, Preparation of polyurethane nanofibers by electrospinning, *J. Appl. Polym. Sci.*, 2008, **109**(1), 406–411.

34 S. Y. Chew, J. Wen, E. K. F. Yim and K. W. Leong, Sustained Release of Proteins from Electrospun Biodegradable Fibers, *Biomacromolecules*, 2005, **6**(4), 2017–2024.

35 S. Budun, E. İşgören, R. Erdem and M. Yüksek, Morphological and mechanical analysis of electrospun

shape memory polymer fibers, *Appl. Surf. Sci.*, 2016, **380**, 294–300.

36 J.-N. Zhang, Y.-M. Ma, J.-J. Zhang, D. Xu, Q.-L. Yang, J.-G. Guan, X.-Y. Cao and L. Jiang, Microfiber SMPU film affords quicker shape recovery than the bulk one, *Mater. Lett.*, 2011, **65**(23), 3639–3642.

37 H. Matsumoto, T. Ishiguro, Y. Konosu, M. Minagawa, A. Tanioka, K. Richau, K. Kratz and A. Lendlein, Shape-memory properties of electrospun non-woven fabrics prepared from degradable polyesterurethanes containing poly(ω-pentadecalactone) hard segments, *Eur. Polym. J.*, 2012, **48**(11), 1866–1874.

38 T. Gong, W. Li, H. Chen, L. Wang, S. Shao and S. Zhou, Remotely actuated shape memory effect of electrospun composite nanofibers, *Acta Biomater.*, 2012, **8**(3), 1248–1259.

39 F. Zhang, Z. Zhang, Y. Liu, H. Lu and J. Leng, The quintuple-shape memory effect in electrospun nanofiber membranes, *Smart Mater. Struct.*, 2013, **22**(8), 085020.

40 K. Gall, C. M. Yakacki, Y. Liu, R. Shandas, N. Willett and K. S. Anseth, Thermomechanics of the shape memory effect in polymers for biomedical applications, *J. Biomed. Mater. Res., Part A*, 2005, **73A**(3), 339–348.

41 C. M. Yakacki, R. Shandas, C. Lanning, B. Rech, A. Eckstein and K. Gall, Unconstrained recovery characterization of shape-memory polymer networks for cardiovascular applications, *Biomaterials*, 2007, **28**(14), 2255–2263.

42 A. Bhargava, *Dynamics of smart materials in high intensity focused ultrasound field*, Virginia Tech, 2020.

43 B. Aarushi, P. Kaiyuan, M. Reza and S. Shima, Ultrasound actuated shape-memory polymer based drug delivery containers, *Proc. SPIE*, 2018, 10595.

44 K. Peng, Y. Zhao, S. Shahab and R. Mirzaeifar, Ductile Shape-Memory Polymer Composite with Enhanced Shape Recovery Ability, *ACS Appl. Mater. Interfaces*, 2020, **12**(52), 58295–58300.

45 G. Jerald Maria Antony, S. Raja, S. T. Aruna and C. S. Jarali, Effect of the addition of diurethane dimethacrylate on the chemical and mechanical properties of tBA-PEGDMA acrylate based shape memory polymer network, *J. Mech. Behav. Biomed. Mater.*, 2020, **110**, 103951.

46 G. Jerald Maria Antony, S. T. Aruna and S. Raja, Enhanced mechanical properties of acrylate based shape memory polymer using grafted hydroxyapatite, *J. Polym. Res.*, 2018, **25**(5), 120.

47 M. Zarek, M. Layani, I. Cooperstein, E. Sachyani, D. Cohn and S. Magdassi, 3D Printing of Shape Memory Polymers for Flexible Electronic Devices, *Adv. Mater.*, 2016, **28**(22), 4449–4454.

48 M. Y. Khalid, Z. U. Arif, R. Noroozi, A. Zolfagharian and M. Bodaghi, 4D printing of shape memory polymer composites: A review on fabrication techniques, applications, and future perspectives, *J. Manuf. Process.*, 2022, **81**, 759–797.

49 H. Wu, P. Chen, C. Yan, C. Cai and Y. Shi, Four-dimensional printing of a novel acrylate-based shape memory polymer using digital light processing, *Mater. Des.*, 2019, **171**, 107704.

50 Y. Y. C. Choong, S. Maleksaeedi, H. Eng, J. Wei and P.-C. Su, 4D printing of high performance shape memory polymer using stereolithography, *Mater. Des.*, 2017, **126**, 219–225.

51 K. Peng and R. Mirzaeifar, Interplay of Chain Orientation and Bond Length in Size Dependency of Mechanical Properties in Polystyrene Nanofibers, *ACS Appl. Polym. Mater.*, 2020, **2**(4), 1664–1671.

52 S.-C. Wong, A. Baji and S. Leng, Effect of fiber diameter on tensile properties of electrospun poly(ε-caprolactone), *Polymer*, 2008, **49**(21), 4713–4722.

53 X. L. Wu, W. M. Huang, H. B. Lu, C. C. Wang and H. P. Cui, Characterization of polymeric shape memory materials, *J. Polym. Eng.*, 2017, **37**(1), 1–20.

54 R. Zhang, S. Wang, J. Tian, K. Chen, P. Xue, Y. Wu and W. Chou, Effect of PEW and CS on the Thermal, Mechanical, and Shape Memory Properties of UHMWPE, *Polymers*, 2020, **12**(2), 483.

55 D. H. Reneker and I. Chun, Nanometre diameter fibres of polymer, produced by electrospinning, *Nanotechnology*, 1996, **7**(3), 216–223.

56 H. Fong, I. Chun and D. H. Reneker, Beaded nanofibers formed during electrospinning, *Polymer*, 1999, **40**(16), 4585–4592.

57 S. Megelski, J. S. Stephens, D. B. Chase and J. F. Rabolt, Micro- and Nanostructured Surface Morphology on Electrospun Polymer Fibers, *Macromolecules*, 2002, **35**(22), 8456–8466.

58 Z. Li and C. Wang, Effects of Working Parameters on Electrospinning, in *One-Dimensional nanostructures: Electrospinning Technique and Unique Nanofibers*, ed. Z. Li and C. Wang, Springer Berlin Heidelberg, Berlin, Heidelberg, 2013, pp. 15–28.

59 F. Abdel-Hady, A. Alzahrany and M. Hamed, Experimental Validation of Upward Electrospinning Process, *ISRN Nanotechnol.*, 2011, **2011**, 851317.

60 T. Sauter, K. Kratz, M. Heuchel and A. Lendlein, Fiber diameter as design parameter for tailoring the macroscopic shape-memory performance of electrospun meshes, *Mater. Des.*, 2021, **202**, 109546.

61 M. Richard-Lacroix and C. Pellerin, Molecular Orientation in Electrospun Fibers: From Mats to Single Fibers, *Macromolecules*, 2013, **46**(24), 9473–9493.

62 P. Chavoshnejad and M. J. Razavi, Effect of the Interfiber Bonding on the Mechanical Behavior of Electrospun Fibrous Mats, *Sci. Rep.*, 2020, **10**(1), 7709.

63 H. R. Han, S. E. Chung and C. H. Park, Shape memory and breathable waterproof properties of polyurethane nanowebs, *Text. Res. J.*, 2012, **83**(1), 76–82.